Appl. Phys. 22, 257–271 (1980)

Applied Physics

On NMR Spin Imaging by Magnetic Field Modulation

L. F. Feiner and P. R. Locher

Philips Research Laboratories, Eindhoven, The Netherlands

Received 4 March 1980/Accepted 31 March 1980

Abstract. A general formalism is presented for the analysis of NMR spin imaging spectra obtained with magnetic field modulation during the free induction decay. We show that weighted integrals of the spin density distribution are measured by this technique and deduce a prescription for reconstructing this distribution from the recorded free induction decay signal. The formalism is applied to two-dimensional imaging with one static and one modulated gradient field. For square-wave and cosine-wave modulation the transformations needed to calculate the image from the spectrum are given explicitly, and their effect is illustrated with computer-simulated pictures. We show how resolution and maximum allowable object size depend on the experimental parameters and argue that even two-dimensional imaging of a 32 cm × 32 cm specimen with a resolution of 1 cm in each direction will be difficult to attain in practice, mainly because of the required strength of the modulated magnetic field.

PACS: 07.58, 76.60, 87.60 G

In recent years a number of different methods for NMR spin imaging have been described which allow the formation of spin density and/or relaxation time images of two- or three-dimensional objects [1–11]. In 1977 Brunner and Ernst [12] made a careful evaluation of the various techniques that were well established by that time. They pointed out that the methods with better sensitivity have a common drawback, namely that the minimum time required for picture formation is rather long: at least several minutes for three-dimensional images and still several seconds for two-dimensional pictures. With reconstruction from projections, for example, many projections must be measured, each requiring about 0.2 s, before a complete picture can be obtained.

To overcome this difficulty Mansfield proposed a new method which he called echo planar imaging [7, 8]. It employs time-dependent magnetic field gradients during the measurement of the free induction decay (FID) signal. With this method it should be possible to obtain a complete picture in the time required for a single FID, which is otherwise needed for the measurement of a single projection. This speed is particularly important for the study of moving objects, as in medical imaging. At the same time the sensitivity of echo planar imaging is expected to be comparable with that of reconstruction from projections, as was noted briefly by Brunner and Ernst. They did not include the technique in their comparison, though, because it was too recent then, and therefore we decided to analyze it in some detail.

The echo planar imaging method in its most simple form may be described as follows. Imaging the spin density distribution in a plane is achieved by the use of two orthogonal magnetic field gradients. One is static, while the gradient direction of the other one is reversed periodically in time. In the absence of these gradients the spectrum obtained from the FID signal would consist of a single line. Its intensity measures the total amount of proton spins in the specimen under study. The static gradient broadens this line into a band of width $\Delta\nu$ which is a projection profile of the spin density along the gradient direction. The other, periodically switched, gradient causes the appearance of sidebands, which are separated from the central band and from each other if the switching frequency exceeds

0340-3793/80/0022/0257/$03.00

$\Delta\nu$. The intensity originally contained in the central band is now distributed over these sidebands in a specific way that reflects the distribution of the spin density in the direction of the switched gradient.

As already indicated by Mansfield, instead of switching one could use other patterns of gradient modulation. What is required is that the gradients in different directions should have a different time dependence so as to make it possible to distinguish the effect of each gradient separately in the measured frequency spectrum. Similar ideas had already been put forward by Hinshaw [13]. The problem is how to extract from the spectrum as much information as possible on the spatial distribution of the spins.

In this paper we present a general formalism for the analysis of NMR spin imaging spectra obtained with magnetic field modulation. It is general to the extent that it can be applied to magnetic fields of arbitrary space and time dependence and thus encompasses the echo planar imaging method. The purpose is to provide a tool both for actually calculating spin density images from such spectra and for assessing the usefulness of various modulation patterns. By way of demonstration we treat two examples with gradient fields in some detail.

The general formalism is described in Sect. 1. We show that what are in fact measured by the present method are weighted integrals of the spin density distribution. Investigation of the weight functions leads to a prescription for reconstructing the image from the recorded FID signal. In Sect. 2 we apply the formalism to two-dimensional imaging with one steady gradient and one time-dependent gradient for the cases of square-wave modulation (gradient switching) and cosine-wave modulation. For both cases explicit formulas are derived for calculating the picture from the spectrum, which take the form of filters to which the spectrum must be subjected. Their effect is demonstrated in computer-simulated pictures, which show the difference between images that are obtained directly from the FID spectrum and images obtained with the reconstructing filter transformations. Section 3 gives the modifications to the formalism that are necessary if the FID signal is sampled instead of recorded continuously. In Sect. 4 we discuss how resolution and maximum allowable object size depend on the experimental parameters. We then make some remarks on the possibilities for practical application by considering a realistic example of two-dimensional imaging in Sect. 5. We summarize our results and conclusions in Sect. 6. Mathematical details have been omitted from the main text as much as possible[1].

[1] For readers interested in proofs and more detailed discussions of various statements made in the text we have prepared three mathematical appendices which can be obtained on request from the first author.

1. General Formalism

We shall discuss an idealized experiment in order to point out the significant features of the image reconstruction problem. For simplicity we shall restrict ourselves to two-dimensional imaging. The generalization to the three-dimensional case is straightforward. Furthermore, the two-dimensional imaging problem itself is of practical interest, e.g. in connection with selective excitation techniques [2, 6, 9, 14].

We thus consider a specimen of finite extension, characterized by a spin density distribution $\varrho(y,z)$ which takes on nonzero values in the region $-Y<y<Y$, $-Z<z<Z$. The specimen is placed in a uniform static magnetic field $\mathbf{B}_0$, let us say in the x direction, i.e. $\mathbf{B}_0=B_0\mathbf{e}_x$, where $\mathbf{e}_x$ is a unit vector. At time $t=0$ a 90° excitation pulse is applied which takes the magnetization $\mathbf{M}$ of the spins into the plane perpendicular to $\mathbf{B}_0$. The free induction decay signal is then observed from $t=0$ until $t=T$ in the presence of two modulation fields $\mathbf{B}_1=B_1(y,t)\mathbf{e}_x$ and $\mathbf{B}_2=B_2(z,t)\mathbf{e}_x$ parallel to the static field.

By quadrature phase-sensitive detection both components of the *rf* magnetization are measured. In the rotating reference frame these components are given by the real and imaginary part of

$$m_+(t)=\int\int \varrho(y,z)\,e^{i\varphi(y,z,t)}\,\lambda(t)\,dy\,dz, \tag{1.1}$$

where

$$\varphi(y,z,t)=\gamma\int_0^t [B_1(y,t')+B_2(z,t')]\,dt'$$
$$=\varphi_1(y,t)+\varphi_2(z,t), \tag{1.2}$$

and

$$\lambda(t)=e^{-t/T_2}. \tag{1.3}$$

In (1.1) $\mathrm{Re}\{m_+(t)\}$ represents the component in the direction along which, throughout the specimen, the magnetization lies immediately after the excitation pulse. Further, γ is the gyromagnetic ratio, $\varphi(y,z,t)$ is the angle through which the magnetization vector has rotated until time t, and $\lambda(t)$ describes transverse relaxation with relaxation time T_2.

It will turn out to be convenient to extend the various functions into the negative time domain. We can assume without loss of generality that the B_i are even functions of time and hence that φ is odd with respect to t. If we furthermore define the relaxation function for $t<0$ by $\lambda(t)\overset{\text{def}}{=}\lambda(-t)$, we must extend the function $m_+(t)$ according to $m_+(t)=m_+(-t)^*$ if we want (1.1) to remain valid for all t. We may suppose that in our idealized experiment the aforementioned direction corresponding to $\mathrm{Re}\{m_+(0)\}$ is known (i.e. we have no phase error) and that the construction of $m_+(t)$ for t

between $-T$ and 0 from the observed behaviour between 0 and T can be performed accurately.

The modulation field B_1 is periodic with circular frequency ω_1. We require that B_1 does not have a time-independent part in order that the phase angle φ_1 returns to zero at the beginning of each period. Further, the effective measuring time $2T$ should be an integral number of periods of B_1. Defining a quantity Ω through $\Omega=\pi/T$ we may express this condition as $\omega_1=M\Omega$, where M is an integer.

As regards to modulation field B_2 we assume at present that it does not exhibit any genuine periodicity. This allows a time-independent B_2 as a special case. We shall demonstrate later (Sect. 4) that the present treatment can easily be extended to the case where the field B_2 is periodic.

Under the stated conditions we can make the following expansions in Fourier series, valid for $-T\leqq t\leqq T$:

$$e^{i\varphi_1(y,t)}=\sum_{n=-\infty}^{\infty}\alpha_n(y)\,e^{in\omega_1 t}, \tag{1.4a}$$

$$\alpha_n(y)=\frac{M}{2T}\int_{-T/M}^{T/M}e^{i\varphi_1(y,t)}e^{-in\omega_1 t}dt, \tag{1.4b}$$

$$e^{i\varphi_2(z,t)}=\sum_{m=-\infty}^{\infty}\beta_m(z)\,e^{im\Omega t}, \tag{1.5a}$$

$$\beta_m(z)=\frac{1}{2T}\int_{-T}^{T}e^{i\varphi_2(z,t)}e^{-im\Omega t}dt. \tag{1.5b}$$

The quantities $\alpha_n(y)$ and $\beta_m(z)$ are real functions and satisfy certain sum rules (Appendix A)[2]. For the moment we neglect relaxation by putting $T_2=\infty$, i.e. $\dot{a}(t)=1$. Substitution of these series in (1.1) and use of $\omega_1=M\Omega$ then yields

$$\begin{aligned}m_+(t)&=\iint\varrho(y,z)\sum_{k=-\infty}^{\infty}\sum_{n=-\infty}^{\infty}\alpha_n(y)\beta_{k-nM}(z)e^{ik\Omega t}dydz\\&=\sum_{k=-\infty}^{\infty}\mathcal{M}_k\,e^{ik\Omega t},\end{aligned} \tag{1.6}$$

with

$$\begin{aligned}\mathcal{M}_k&=\frac{1}{2T}\int_{-T}^{T}m_+(t)\,e^{-ik\Omega t}dt\\&=\iint\varrho(y,z)\Phi_k(y,z)dydz,\end{aligned} \tag{1.7}$$

$$\Phi_k(y,z)=\sum_{n=-\infty}^{\infty}\alpha_n(y)\beta_{k-nM}(z). \tag{1.8}$$

We see from (1.7) that the spectrum of $m_+(t)$ yields weighted integrals $\mathcal{M}_k$ of $\varrho(y,z)$ with respect to the set of weight functions $\{\Phi_k(y,z)\}$. The information on the spin density distribution that is contained in these integrals depends upon the weight functions. It is important to note that the latter are completely determined by the modulation fields B_1 and B_2, which therefore determine ultimately what kind of information about $\varrho(y,z)$ we obtain. Naturally, in practice the choice of the modulation fields will be a compromise between demands of simple realization of the B_i and of useful information in the $\mathcal{M}_k$. We remark that only for some very special $\{\Phi_k\}$, i.e. for very special choices of the modulation fields, will it occur that each weighted integral $\mathcal{M}_k$ corresponds to a separate area element in the specimen.

It is most convenient if $\{\Phi_k(y,z)\}$ is an orthonormal set of functions,

$$\iint\Phi_k(y,z)\Phi_l(y,z)dydz=\delta_{kl}, \tag{1.9}$$

for in that case we can immediately represent our information on the spin density by

$$\varrho(y,z)\approx\sum_{k=-\infty}^{\infty}\mathcal{M}_k\Phi_k(y,z). \tag{1.10}$$

The "approximately equal" sign is used here because the set $\{\Phi_k(y,z)\}$ will in general not be complete, and indicates that the right-hand side of (1.10) represents $\varrho(y,z)$ only to the extent that it correctly reproduces the weighted integrals $\mathcal{M}_k$. The equality sign would require

$$\sum_{k=-\infty}^{\infty}\Phi_k(y,z)\Phi_k(y',z')=\delta(y-y')\delta(z-z'), \tag{1.11}$$

and the better this completeness relation is *approximately* fulfilled by the $\Phi_k(y,z)$, the better $\varrho(y,z)$ is represented by (1.10).

In general, the weight functions $\Phi_k(y,z)$ are neither orthogonal nor complete. However, nonorthogonality poses no serious additional problems, since it is always possible, at least in principle, to construct an orthonormal set $\{\tilde{\Phi}_k(y,z)\}$ from the $\Phi_k(y,z)$ by Schmidt's orthogonalization [15],

$$\tilde{\Phi}_k(y,z)=\sum_l\tilde{S}_{kl}\Phi_l(y,z), \tag{1.12}$$

$$\iint\tilde{\Phi}_k(y,z)\tilde{\Phi}_l(y,z)dydz=\delta_{kl}. \tag{1.13}$$

The spin density is then expanded in terms of these functions as

$$\varrho(y,z)\approx\sum_k\tilde{\mathcal{M}}_k\tilde{\Phi}_k(y,z), \tag{1.14}$$

where

$$\tilde{\mathcal{M}}_k=\iint\varrho(y,z)\tilde{\Phi}_k(y,z)dydz=\sum_l\tilde{S}_{kl}\mathcal{M}_l, \tag{1.15}$$

in order that the weighted integrals produced by the right-hand side of (1.14) are in agreement with (1.7). The representation of the spin density by (1.14) is then accurate to the same degree as $\{\tilde{\Phi}_k(y,z)\}$ comes close to being a complete set, and this in turn depends on what the $\Phi_k(y,z)$ are and therefore on the modulation fields.

An alternative to Schmidt's orthogonalization, which turns out to be easier in the cases to be studied in the

[2] See footnote on p. 258.

next section, is to construct a biorthonormal system from the $\Phi_k(y,z)$. It amounts to the following prescription for reconstructing the spin density distribution from the $\mathcal{M}_k$.

Construct two sets of functions $\{\Psi_j(y,z)\}$ and $\{X_j(y,z)\}$ which satisfy

$$\text{(i)} \quad X_j(y,z)=\sum_k S_{jk}\Phi_k(y,z), \tag{1.16}$$

which states that the X_j are linear combinations of the Φ_k,

$$\text{(ii)} \quad \iint \Psi_k(y,z)X_j(y,z)dydz=\delta_{kj}, \tag{1.17}$$

so that the two sets form a biorthonormal system, and

$$\text{(iii)} \quad \sum_j \Psi_j(y,z)X_j(y',z')=\Delta(y'-y,z'-z), \tag{1.18}$$

where the function $\Delta(y'',z'')$ is strongly peaked near $(0,0)$, so that the two sets approximate a complete function system [for exact completeness $\Delta(y'',z'')$ should be a two-dimensional Dirac delta function as in the right-hand side of (1.11)]. Then transform the spectrum according to

$$\mathcal{P}_j=\sum_k S_{jk}\mathcal{M}_k, \tag{1.19}$$

and the optimal representation of the spin density distribution is given by

$$\varrho'(y,z)=\sum_j \mathcal{P}_j\Psi_j(y,z). \tag{1.20}$$

Since the reconstructed density $\varrho'(y,z)$ obtained by this procedure is related to the true density $\varrho(y,z)$ by

$$\varrho'(y,z)=\iint\varrho(y+y'',z+z'')\Delta(y'',z'')dy''dz'', \tag{1.21}$$

variations in $\varrho(y,z)$ on a scale smaller than the width of $\Delta(y'',z'')$ will appear smoothed in $\varrho'(y,z)$ but the more gradual variations in spin density are represented faithfully by the reconstruction. In the next section we shall demonstrate that the required construction of the sets $\{\Psi_j\}$ and $\{X_j\}$ can actually be carried through for a wide class of modulation fields.

We now briefly consider the consequences of relaxation, i.e. T_2 finite. The relaxation function can be expanded in the interval $[-T,T]$,

$$s(t)=\sum_{l=-\infty}^{\infty}\mathcal{R}_l(T/T_2)\,e^{il\Omega t}, \tag{1.22a}$$

$$\mathcal{R}_l(T/T_2)=\frac{1}{2T}\int_{-T}^{T}e^{-|t|/T_2}e^{-il\Omega t}dt$$

$$=\frac{T}{T_2}\cdot\frac{1-(-1)^l e^{-T/T_2}}{l^2\pi^2+(T/T_2)^2}, \tag{1.22b}$$

and one finds that $\mathcal{M}_k$ is replaced in (1.6) by

$$\mathcal{M}'_k=\sum_{l=-\infty}^{\infty}\mathcal{M}_{k-l}\mathcal{R}_l(T/T_2). \tag{1.23}$$

So the relaxational broadening of the spectrum intermixes the weighted integrals in a Lorentz-like pattern. This effect is minimized if T/T_2 is as small as possible.

2. Gradient Modulation

We shall treat two specific examples by the formalism just developed. The first one is gradient switching, which was discussed by Mansfield [7, 8] in some detail. The second one is cosine-wave gradient modulation, which he mentioned briefly.

We thus take modulation fields that are linear gradient fields. Moreover we assume that B_2 is actually not modulated at all but is steady. It is then convenient to write

$$B_1(y,t)=G_y y f_1(t), \tag{2.1}$$

$$B_2(z,t)=G_z z, \tag{2.2}$$

so as to separate the dependence on time from the dependence on position in B_1. We choose the function $f_1(t)$ to have maximum modulus equal to 1. Then G_y and G_z characterize the strength of the gradient fields, and we introduce $y_0=\omega_1/\gamma G_y$ and $z_0=\Omega/\gamma G_z$ as fundamental units of length in the y and z direction, respectively.

For definiteness we shall assume from now on that M is odd, and write $M=2M'+1$. An even value of M would make some equations slightly more complicated but all results would be essentially just the same as in the case of odd M described below.

For the field given by (2.2) the functions introduced in (1.5b) are

$$\beta_m(z)=\frac{\sin[\pi(z-mz_0)/z_0]}{\pi(z-mz_0)/z_0}=w_m(z/z_0). \tag{2.3}$$

One may verify that for these functions there exists the relation

$$\beta_m(-z)=\beta_{-m}(z), \tag{2.4}$$

and that they satisfy the addition theorem

$$\sum_{k=-\infty}^{\infty}\beta_{m-k}(z)\beta_k(z')=\beta_m(z+z'). \tag{2.5}$$

These properties derive directly from the gradient form of the modulation field (Appendix A)[3]. Consequently, equations quite analogous to (2.4) and (2.5) hold for the functions $\alpha_n(y)$ introduced in (1.4b). Actually, for the $\alpha_n(y)$ (2.4) can be extended to

$$\alpha_n(-y)=\alpha_{-n}(y)=(-1)^n\alpha_n(y), \tag{2.6}$$

[3] See footnote on p. 258.

because of the particular symmetry

$$f_1(t+\pi/\omega_1) = -f_1(t) \tag{2.7}$$

that is implied both by switching and by cosine-wave modulation.

2.1. Square Wave Modulation (Gradient Switching)

The modulation pattern proposed by Mansfield is obtained by reversing the y gradient at times that are an odd multiple of a time interval τ:

$${}_{\mathrm{S}}f_1(t) = \begin{cases} +1 & \text{if} \quad -\tau + l4\tau < t < \tau + l4\tau \\ -1 & \text{if} \quad \tau + l4\tau < t < 3\tau + l4\tau \end{cases}$$
$$(l \text{ integer}), \tag{2.8}$$

the left subscript S standing for square-wave modulation. Note that τ is a quarter period of $f_1(t)$, $4\tau = 2\pi/\omega_1$. We now find

$${}_{\mathrm{S}}\alpha_n(y) = \frac{1}{2}\left[\frac{\sin[\pi(y-ny_0)/2y_0]}{\pi(y-ny_0/2y_0)} + (-1)^n \frac{\sin[\pi(y+ny_0)/2y_0]}{\pi(y+ny_0)/2y_0}\right] = v_n(y/2y_0). \tag{2.9}$$

In the present case one can derive a closed expression for the functions ${}_{\mathrm{S}}\Phi_k(y,z)$ but the resulting formula is rather formidable, and we shall therefore try to appreciate the essential features of these functions without actually calculating them. To this end consider a function ${}_{\mathrm{S}}\Phi_k(y,z)$ with a particular value of k which we write as $k = nM + m$ with m uniquely determined by the requirement $-M' \leqq m \leqq M'$. Then

$$\begin{aligned} {}_{\mathrm{S}}\Phi_{nM+m}(y,z) &= \sum_{l=-\infty}^{\infty} {}_{\mathrm{S}}\alpha_l(y)\beta_{m+(n-l)M}(z) \\ &= \ldots + {}_{\mathrm{S}}\alpha_{n-1}(y)\beta_{m+M}(z) + {}_{\mathrm{S}}\alpha_n(y)\beta_m(z) \\ &\quad + {}_{\mathrm{S}}\alpha_{n+1}(y)\beta_{m-M}(z) + \ldots . \end{aligned} \tag{2.10}$$

We now use the fact that the specimen has finite size: if half its length Z is sufficiently smaller than $M'z_0$, out of the various $\beta_p(z)$ appearing in (2.10) only $\beta_m(z)$ will differ appreciably from zero within the extension of the specimen. As regards the value of ${}_{\mathrm{S}}\mathcal{M}_{nM+m}$ we may therefore say that we have effectively

$${}_{\mathrm{S}}\Phi_{nM+m}(y,z) \approx {}_{\mathrm{S}}\alpha_n(y)\beta_m(z) = v_n(y/2y_0)w_m(z/z_0), \quad m = -M', \ldots, M', \quad n = -\infty, \ldots, \infty. \tag{2.11}$$

In this approximation functions with opposite values of n are identical in view of (2.6).

The first observation we can make from (2.3), (2.9), and (2.11) is, that nuclear spins in an area element of approximate size $2y_0 \times z_0$ and centered at (ny_0, mz_0) contribute mainly to ${}_{\mathrm{S}}\mathcal{M}_{nM+m}$ and ${}_{\mathrm{S}}\mathcal{M}_{-nM+m}$, or conversely, that ${}_{\mathrm{S}}\mathcal{M}_{nM+n}$ acquires its predominant contributions both from spins in the neighbourhood of (ny_0, mz_0) and from spins near $(-ny_0, mz_0)$. We may understand this as follows. In these two area elements the spins experience a y gradient field which makes them precess with a circular frequency that alternates between $ny_0\gamma G_y = n\omega_1 = nM\Omega$ and $-n\omega_1$. This precession always has opposite phase in the two regions. In addition all these spins experience the same z gradient field, which increases their circular precession frequency by $mz_0\gamma G_z = m\Omega$. Therefore, the spins in *both* area elements, although with different phase, alternately precess with circular frequencies $(nM+m)\Omega$ *and* $(-nM+m)\Omega$.

The implication is that ${}_{\mathrm{S}}\mathcal{M}_k$ as a function of k (i.e. of frequency) does not directly provide a line-by-line scan of the spin density distribution as was suggested by Mansfield. That assumption in fact leads to spurious reflections in the picture which render it impossible to distinguish between regions with opposite y coordinate. This is illustrated by the results of a computer simulation shown in Figs. 1a and b. Simulated is the situation where there is a single spot of spin density at position $(4y_0, 4z_0)$. The Fourier transform of the resulting FID signal is shown in Fig. 1a. If this spectrum is converted into a line-by-line intensity plot on the (erroneous) assumption that $\varrho(ny_0, mz_0) \propto {}_{\mathrm{S}}\mathcal{M}_{nM+m}$, Fig. 1b is obtained, in which z increases from left to right, y from top to bottom. In addition to the bright spot at the correct position in the lower half of the picture, there is a bright feature in the upper half around the position $(-4y_0, 4z_0)$.

Our second observation is that it is actually possible to obtain a representation where each coefficient may be identified with the spin density in a single small area and that this can be achieved by a simple and exactly calculable transformation of the spectrum. To see this we should realize that $\{w_m(x)\}$ is a set of orthogonal functions in the variable x. According to (2.11) the z-dependent factor in ${}_{\mathrm{S}}\Phi_{nM+m}(y,z)$ is already such a function, the width z_0 of any individual function being equal to the separation between the maxima of successive functions. On the other hand the two terms in ${}_{\mathrm{S}}\alpha_n(y)$ [see (2.9)] that make up the y-dependent part in ${}_{\mathrm{S}}\Phi_{nM+m}(y,z)$ have an individual width equal to $2y_0$ while corresponding terms in successive ${}_{\mathrm{S}}\alpha_n(y)$ have their maxima only y_0 apart, which is too close for such terms to be independent. Therefore the terms with their maximum at an odd multiple of y_0 can be expressed in those with their maximum at an even multiple of y_0 and vice versa. By doing so we can construct a set of independent functions with a single maximum at either a positive or a negative multiple of $2y_0$.

We proceed to the precise mathematical formulation of the above. We choose the following functions as the

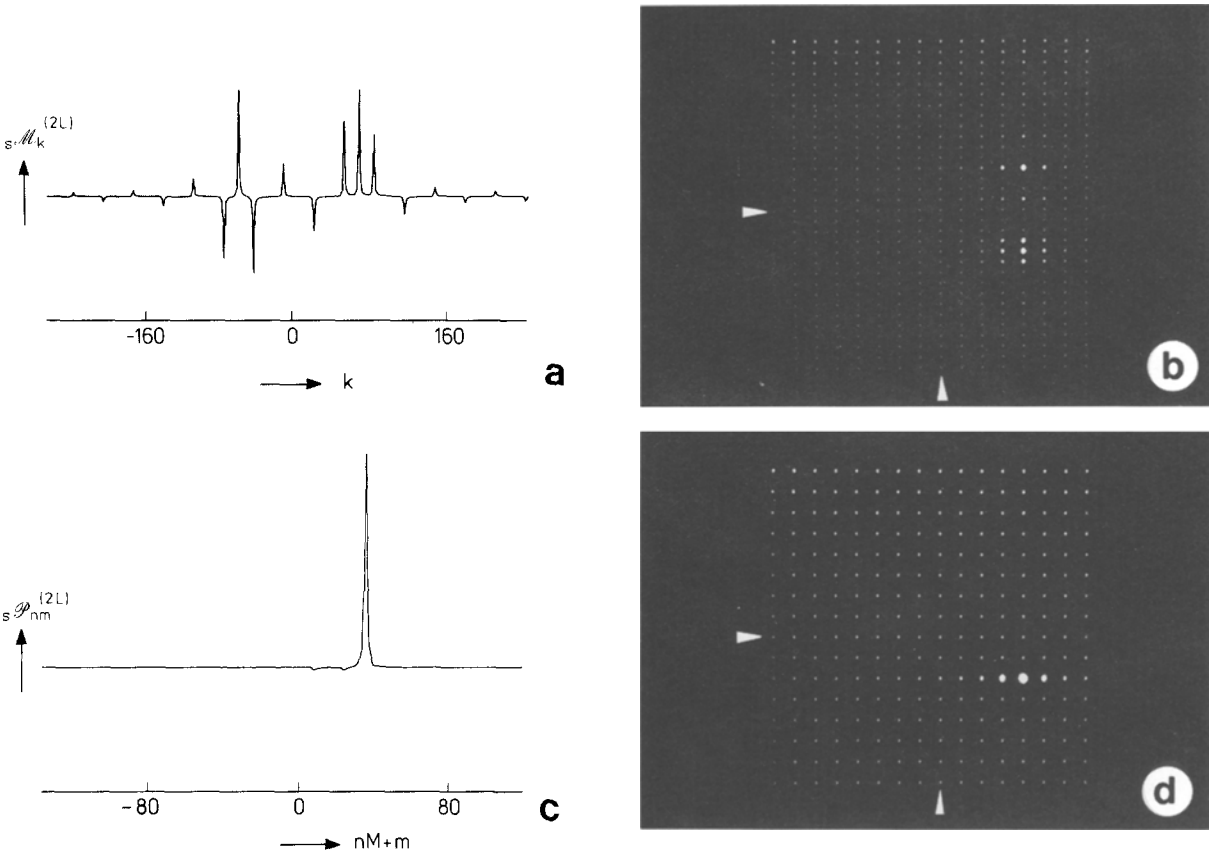

Fig. 1a–d. Computer simulation of image formation with one static and one square-wave modulated magnetic gradient field. Expressed in the time unit for which the sample rate is equal to 1 the example shown has $T=256$, $4\tau=32$, and $T_2=128$, so $N=M=16$. Simulated is the presence of a single spot of spin density at position $(4y_0, 4z_0)$: (a) spectral coefficients ${}_s\mathscr{M}_k^{(2L)}$ as a function of k (frequency), (b) line-by-line intensity plot of $\{|{}_s\mathscr{M}_{nM+m}^{(2L)}| - 16 \leqq n \leqq 15;\ -8 \leqq m \leqq 7\}$, (c) transformed coefficients ${}_s\mathscr{P}_{nm}^{(2L)}$ versus $nM+m$, (d) intensity plot of $\{|{}_s\mathscr{P}_{nm}^{(2L)} = 2y_0 z_0\ {}_s\bar{\varrho}(n2y_0, mz_0)| - 8 \leqq n \leqq 7;\ -8 \leqq m \leqq 7\}$. In (b) and (d) m increases from left to right, corresponding to the z direction, n from top to bottom, corresponding to the y direction, and the arrows indicate the origin

set to expand the spin density in

$$ {}_s\Psi_{nm}(y,z) = w_n(y/2y_0 + (z/z_0 - m)/2M)\, w_m^{(M)}(z/z_0)\,, \qquad m = -M', \ldots, M', \quad n = -\infty, \ldots, \infty\,, \tag{2.12} $$

where the function with superscript (M) is defined as

$$ w_m^{(M)}(z/z_0) = \sum_{l=-\infty}^{\infty} w_{m+lM}(z/z_0) = \frac{\sin[\pi(z - mz_0)/z_0]}{M \sin[\pi(z - mz_0)/Mz_0]}\,. \tag{2.13} $$

The functions ${}_s\Psi_{nm}(y,z)$ are related to the functions ${}_s\Phi_k(y,z)$ [as given by (2.10), not approximated according to (2.11)] by

$$ {}_s\Psi_{nm}(y,z) = {}_s\Phi_{2nM+m}(y,z) + \sum_{n'=-\infty}^{\infty} S_{nn'}\, {}_s\Phi_{(2n'-1)M+m}(y,z)\,, \tag{2.14a} $$

$$ S_{nn'} = \frac{(-1)^{n-n'}}{(n-n'+\frac{1}{2})\pi} = w_0(n-n'+\tfrac{1}{2})\,. \tag{2.14b} $$

Therefore

$$ {}_s\mathscr{P}_{nm} \overset{\text{def}}{=} \iint \varrho(y,z)\, {}_s\Psi_{nm}(y,z)\,dy\,dz = {}_s\mathscr{M}_{2nM+m} + \sum_{n'=-\infty}^{\infty} S_{nn'}\, {}_s\mathscr{M}_{(2n'-1)M+m}\,, \tag{2.15} $$

and this transformation is called a filtering of the spectrum. Since the ${}_s\Psi_{nm}(y,z)$ are orthogonal functions on the strip $-\infty < y < \infty$, $-Mz_0/2 \leqq z \leqq Mz_0/2$, the spin density distribution is then represented by

$$ {}_s\varrho(y,z) = \frac{1}{2y_0 z_0} \sum_{n=-\infty}^{\infty} \sum_{m=-M'}^{M'} {}_s\mathscr{P}_{nm}\, {}_s\Psi_{nm}(y,z)\,, \tag{2.16} $$

which is unambiguous if the specimen dimensions are such that $Z < Mz_0/2$.

The functions used in this expansion have some nice properties which are reflected in ${}_s\varrho(y,z)$. Besides being orthogonal the set $\{{}_s\Psi_{nm}(y,z)\}$ is what we call semi-complete: it is complete on the discrete lattice with spacing $2y_0$ in the y direction and z_0 in the z direction. It is therefore capable of representing faithfully any

smooth function on the afore mentioned strip, apart from details smaller than $2y_0 \times z_0$. On the lattice the set is also orthonormal with respect to a discrete inner product and its members are the natural basis vectors, i.e. at the lattice point $(n2y_0, mz_0)$ the function with corresponding indices has the value one while all other functions are zero there.

The semicompleteness implies

$$ {}_S\varrho(y,z) = \frac{1}{2y_0 z_0} \iint \varrho(y+y', z+z') \cdot w_0(y'/2y_0 + z'/2Mz_0) w_0^{(M)}(z'/z_0) dy' dz' , \quad (2.17) $$

which shows ${}_S\varrho(y,z)$ to be a smoothed $\varrho(y,z)$. The smoothing roughly has the effect of removing from $\varrho(y,z)$ all (spatial) frequencies higher than $1/2y_0$ and $1/z_0$ in the reciprocal y direction and z direction, respectively, but the resulting ${}_S\varrho(y,z)$ still contains complete information on the more gradual variations in the spin density (Appendix B)[4]. The values assumed by ${}_S\varrho(y,z)$ at the lattice points $(n2y_0, mz_0)$ are precisely the expansion coefficients in (2.16) and therefore characterize the function completely.

The effect of the transformation is further illustrated by the computer simulation results in Figs. 1c and d. The filter given by (2.15) was applied to the spectrum of Fig. 1a and the result is shown in Fig. 1c. Conversion into an intensity plot according to ${}_S\varrho(n2y_0, mz_0) \propto {}_S\mathscr{P}_{nm}$ gives Fig. 1d. The spurious feature in the upper half of the picture has now disappeared: there is only a bright spot at the correct position $(4y_0, 4z_0)$. We remark that only the independent data points are shown here. For a good visual impression of the image it will be necessary to include a number of intermediate points.

We have seen that square-wave modulation of the gradient fields yields a signal that admits a rather straightforward interpretation. After a simple transformation necessary to remove spurious reflections the filtered spectrum $\{{}_S\mathscr{P}_{nm}\}$ represents the spin density at successive points of an equidistant lattice, and determines the low-(spatial)-frequency part of the density in between as well. The dominant contributions to a particular ${}_S\mathscr{P}_{nm}$ come from only a few ${}_S\mathscr{M}_{n'M+m'}$ in the original spectrum, viz. those with $m' = m$, $n' \approx 2n$.

It is now easy to interpret the effect of relaxation. The contamination of each coefficient ${}_S\mathscr{M}_{nM+m}$ with its neighbours, described by (1.23), produces smoothing of ${}_S\varrho(y,z)$ over successive lattice points and therefore loss of resolution in the z direction. This has curious consequences near the edges. If m is slightly smaller than M' the coefficient ${}_S\mathscr{M}_{2nM+m}$, which would mainly contribute to ${}_S\mathscr{P}_{nm}$, contaminates coefficients ${}_S\mathscr{M}_{(2n+1)M+m'}$ within m' slightly larger than $-M'$ and these contribute predominantly to ${}_S\mathscr{P}_{nm'}$ and ${}_S\mathscr{P}_{n+1,m'}$, that is at the other edge of the image.

One may say that the use of the filter doubles the amount of information that is extracted from the signal. This may be appreciated from the following argument. Without the transformation we would only obtain a well defined image from the ${}_S\mathscr{M}_{nM+m}$ if we took care that $\varrho(y,z)$ were zero for negative y so that reflections could not give rise to any ambiguity. Seemingly the ensuing loss in allowable specimen size would be compensated for by the finer resolution in the y direction: without the transformation y_0 as compared to $2y_0$ with the transformation. However, if $\varrho(y,z) = 0$ for $y < 0$ the ${}_S\mathscr{M}_{nM+m}$ with odd n do not contain any information that is independent of the information in the ${}_S\mathscr{M}_{nM+m}$ with even n, and the resolution is still effectively $2y_0$. Therefore the effect of the filter is, so to speak, to make the region $y < 0$ available for the specimen without any loss in resolution.

Single-phase detection of the signal produces an artefact in the form of an inversion of the image (including spurious reflections if present) through the origin. This cannot be remedied by mathematical means and an unambiguous image is obtained only if $\varrho(y,z) = 0$ in a halfspace, say for $z < 0$. Hence there is a loss in the possible specimen size by a factor of two (four if the transformation is also omitted) which is consistent with the number of data being halved compared with quadrature detection.

It appears from (2.14a) that the set $\{{}_S\Psi_{nm}\}$ contains in a way only half as many functions as the set $\{{}_S\Phi_k\}$, since there is a one-to-one correspondence between the functions ${}_S\Phi_{nM+m}$ with *even* n only and the functions belonging to the set $\{{}_S\Psi_{nm}\}$. One might thus wonder whether an independent second set can be constructed from $\{{}_S\Phi_k\}$. Actually this is possible by replacement of the plus sign by a minus sign in (2.14a) from which an orthogonal set $\{{}_S\Psi^1_{nm}\}$ results. The functions from this set are not dependent on the functions ${}_S\Psi_{nm}$ obtained with the plus sign, but they are also not orthogonal to them. It may be shown (Appendix C)[5] that if both $\{{}_S\Psi_{nm}\}$ *and* $\{{}_S\Psi^1_{nm}\}$ are used, the spin density can in principle be reconstructed on a strip that is twice as broad in the z direction as is possible with $\{{}_S\Psi_{nm}\}$ alone, with the same resolution $2y_0 \times z_0$ as in that case. For that purpose the sets $\{{}_S\Psi_{nm}\}$ and $\{{}_S\Psi^1_{nm}\}$ (or the weighted integrals corresponding to them) must be disentangled because of their non-orthogonality. This necessarily involves a procedure equivalent to solving linear equations with a matrix that is very ill-conditioned. This is connected with the fact that the set $\{{}_S\Phi_k\}$ contains pairs of functions that are approximate-

[4] See footnote on p. 258.

[5] See footnote on p. 258.

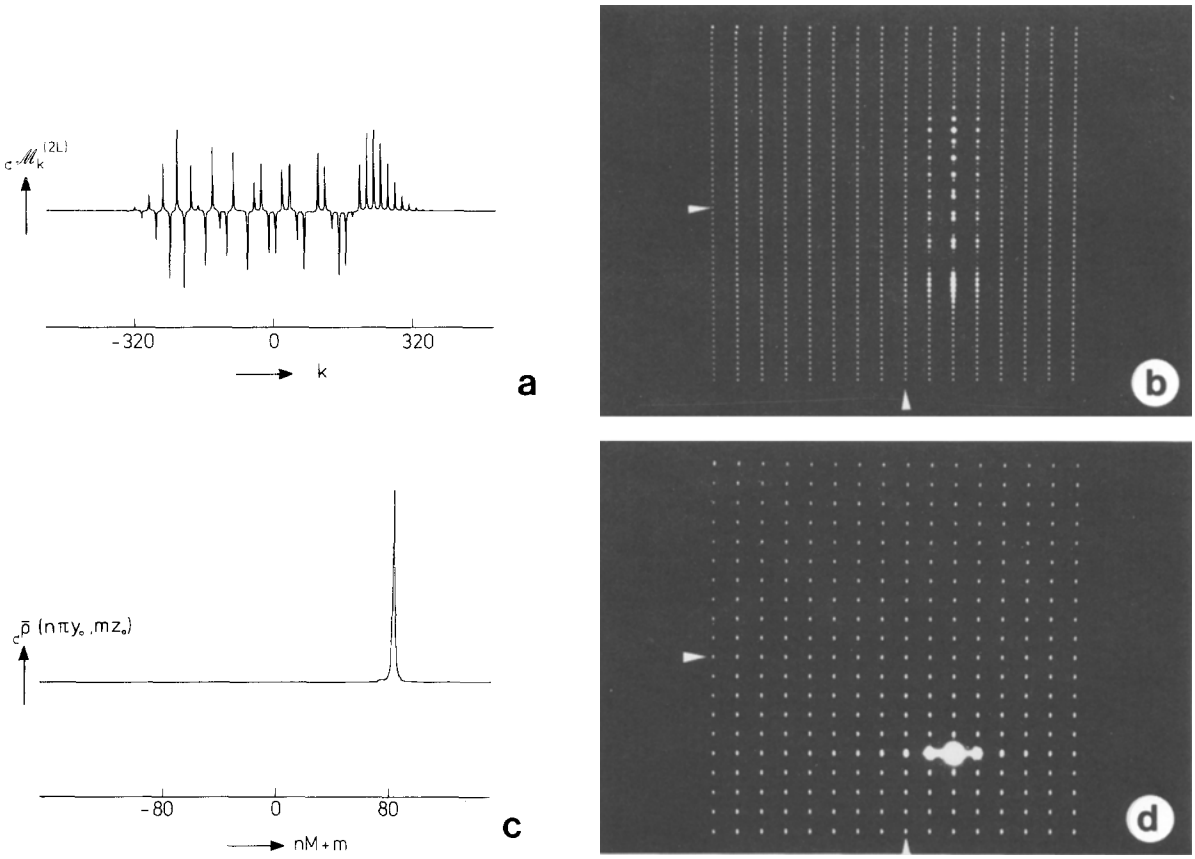

Fig. 2a–d. Computer simulation of image formation with one static and one cosine-wave modulated magnetic gradient field. Expressed in the time unit for which the sample rate is equal to 1 the example shown has $T=512$, $2\pi/\omega_1=64$, and $T_2=256$ so $N=32$, $M=16$. Simulated is the presence of a single spot of spin density at position $(5\pi y_0, 2z_0)$: (a) spectral coefficients ${}_C\mathcal{M}_k^{(2L)}$ as a function of k (frequency), (b) line-by-line intensity plot of $\{{}_C\mathcal{M}_{nM+m}^{(2L)}| -32\leqq n\leqq 31;\ -8\leqq m\leqq 7\}$, (c) transformed values ${}_C\bar{\varrho}(n\pi y_0, mz_0)$ versus $nM+m$, (d) intensity plot of $\{{}_C\bar{\varrho}(n\pi y_0, mz_0)| -10\leqq n\leqq 9;\ -8\leqq m\leqq 7\}$. In (b) and (d) m increases from left to right, corresponding to the z direction, n from top to bottom, corresponding to the y direction, and the arrows indicate the origin

ly dependent, as we noticed after (2.11). The problem can only be circumvented if resolution in the y direction is given up to a considerable extent. So in practice the penalty for an increase of the allowable specimen size in one direction is loss of resolution in the other direction.

2.2. Cosine Wave Modulation

Since switching a gradient field at high frequency may pose serious practical difficulties it is of particular interest to consider the replacement of the square wave form by a cosine-wave modulation pattern for the y gradient,

$$ {}_Cf_1(t)=\cos(\omega_1 t). \tag{2.18}$$

In this case one finds

$$ {}_C\alpha_n(y)=J_n(y/y_0). \tag{2.19}$$

where $J_n(\cdot)$ is a Bessel function [16].

For a discussion we again content ourselves with establishing by the same reasoning as before that one has to a good approximation

$$ {}_C\Phi_{nM+m}(y,z)\approx {}_C\alpha_n(y)\beta_m(z)=J_n(y/y_0)w_m(z/z_0), \quad m=-M',\ldots,M', \quad n=-\infty,\ldots,\infty. \tag{2.20}$$

Again functions with opposite n are identical in this approximation, because the Bessel functions satisfy (2.6).

Our first observation is that, by the very nature of the Bessel functions, spins in the neighbourhood of (ny_0, mz_0) contribute predominantly to all coefficients ${}_C\mathcal{M}_{n'M+m}$ with $|n'|\lesssim|n|$, or conversely that ${}_C\mathcal{M}_{nM+m}$ acquires significant contributions from spins in the two half strips along (y, mz_0) with $|y|\gtrsim|n|y_0$. This is understandable if one considers that spins close to (ny_0, mz_0) experience a y gradient field which makes them precess with a circular frequency that is gradually modulated between $ny_0\gamma G_y=n\omega_1=nM\Omega$ and $-n\omega_1$. It is clear that no simple relation exists between well delimited area elements in the specimen and particular coef-

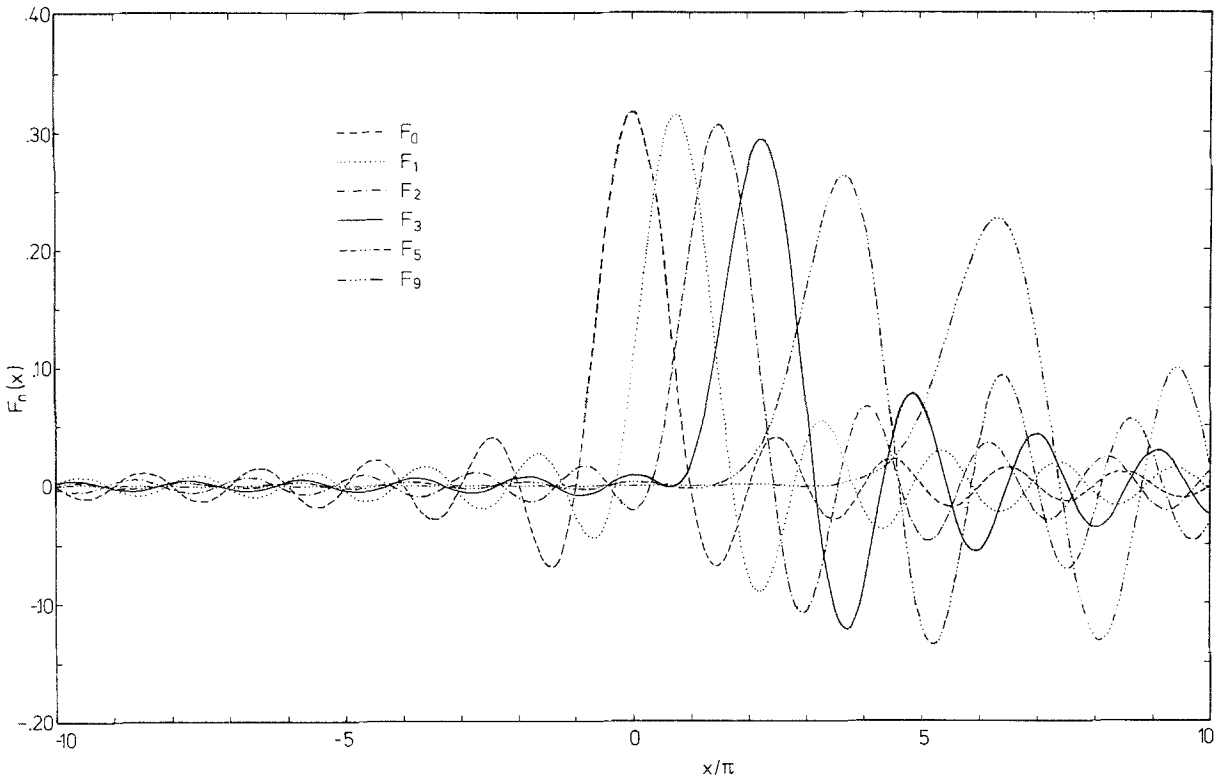

Fig. 3. The functions $F_n(x)$ for $n=0, 1, 2, 3, 5, 9$

ficients in the spectrum. Certainly ${}_C\mathcal{M}_k$ as a function of k can not even resemble a line-by-line scan of the spin density distribution.

This is demonstrated in Figs. 2a and b where results of computer simulation are shown, analogous to those for the square-wave case. Figure 2a shows the Fourier transform of the FID signal that is produced by a single spot of spin density at position $(5\pi y_0, 2z_0)$. When converted into an intensity plot as if $\varrho(ny_0, mz_0) \propto {}_C\mathcal{M}_{nM+m}$ it yields Fig. 2b. From the bright spot at the correct position in the lower half of the picture a complicated spurious feature emerges, which extends roughly to the opposite point in the upper half of the picture.

The second observation we make is that the structure of the functions ${}_C\Phi_k(y,z)$ is very similar to that of the ${}_S\Phi_k(y,z)$. This enables us to reconstruct the spin density by proceeding in close analogy with what we did in the square-wave case.

For that purpose we must introduce two sets of functions

$$
\begin{aligned}
{}_CX_{nm}(y,z) &= \sum_{l=-\infty}^{\infty} K_{n+l/2}(y/y_0) w_{m-lM}(z/z_0) \\
&= K_{n-(z/z_0-m)/2M}(y/y_0) w_m^{(M)}(z/z_0), \\
& m = -M', \ldots, M', \quad n = -\infty, \ldots, \infty, \qquad (2.21)
\end{aligned}
$$

and

$$
\begin{aligned}
{}_C\Psi_{nm}(y,z) &= \sum_{l=-\infty}^{\infty} F_{n+l/2}(y/y_0) w_{m-lM}(z/z_0) \\
&= F_{n-(z/z_0-m)/2M}(y/y_0) w_m^{(M)}(z/z_0), \\
& m = -M', \ldots, M', \quad n = -\infty, \ldots, \infty. \qquad (2.22)
\end{aligned}
$$

The functions $K_\nu(\cdot)$ and $F_\nu(\cdot)$ that appear here are defined by an integral representation for arbitrary real values of the order ν (Appendix B)[6], but for half-integer order they can be expressed as a series of Bessel functions:

$$
K_{n/2}(x) = J_n(x) + \sum_{l=-\infty}^{\infty} \frac{(-1)^l}{(l+\frac{1}{2})\pi} J_{n+2l+1}(x), \qquad (2.23)
$$

$$
\begin{aligned}
F_{n/2}(x) &= \frac{1}{4}[J_{n-1}(x) + J_{n+1}(x)] \\
&\quad + \sum_{l=-\infty}^{\infty} \frac{(-1)^l}{(1-4l^2)\pi} J_{n+2l}(x). \qquad (2.24)
\end{aligned}
$$

Equations (2.23) and (2.24) are useful for numerical calculation of these functions since the series converge rapidly and fast numerical procedures for calculating Bessel functions are available. In Fig. 3 we show some

[6] See footnote on p. 258.

$F_\nu(x)$ of integer order. The functions ${}_{\mathrm{C}}X_{nm}(y,z)$ are related to the functions ${}_{\mathrm{C}}\Phi_k(y,z)$ by

$$ {}_{\mathrm{C}}X_{nm}(y,z) = {}_{\mathrm{C}}\Phi_{2nM+m}(y,z) + \sum_{n'=-\infty}^{\infty} S_{nn'}\, {}_{\mathrm{C}}\Phi_{(2n'-1)M+m}(y,z) \tag{2.25} $$

with the same coefficients $S_{nn'}$ given by (3.14b) as we had in the square-wave case. Thus

$$ {}_{\mathrm{C}}\mathscr{P}_{nm} \overset{\mathrm{def}}{=} \iint \varrho(y,z)\, {}_{\mathrm{C}}X_{nm}(y,z)\,dy\,dz = {}_{\mathrm{C}}\mathscr{M}_{2nM+m} + \sum_{n'=-\infty}^{\infty} S_{nn'}\, {}_{\mathrm{C}}\mathscr{M}_{(2n'-1)M+m} \tag{2.26} $$

and since the sets $\{{}_{\mathrm{C}}\Psi_{nm}\}$ and $\{{}_{\mathrm{C}}X_{nm}\}$ form a biorthogonal system on the strip $-\infty<y<\infty$, $-Mz_0/2 \leqq z \leqq Mz_0/2$, the spin density distribution is represented by

$$ {}_{\mathrm{C}}\varrho(y,z) = \frac{1}{y_0 z_0} \sum_{n=-\infty}^{\infty} \sum_{m=-M'}^{M'} {}_{\mathrm{C}}\mathscr{P}_{nm}\, {}_{\mathrm{C}}\Psi_{nm}(y,z), \tag{2.27} $$

which is unambiguous if the size of the specimen is such that $Z<Mz_0/2$.

Similar to the former case, the biorthogonal system made up by $\{{}_{\mathrm{C}}\Psi_{nm}\}$ and $\{{}_{\mathrm{C}}X_{nm}\}$ is semicomplete too, namely with respect to the discrete lattice with spacing πy_0 in the y direction and z_0 in the z direction. The system is also biorthogonal with respect to a discrete inner product on that lattice, but the ${}_{\mathrm{C}}\Psi_{nm}(y,z)$ are not the natural basis vectors.

It follows from the semicompleteness that

$$ {}_{\mathrm{C}}\varrho(y,z) = \frac{1}{y_0 z_0} \iint \varrho(y+y', z+z') \cdot F_{-z'/2Mz_0}(y'/y_0)\, w_0^{(M)}(z'/z_0)\,dy'\,dz'. \tag{2.28} $$

This implies that ${}_{\mathrm{C}}\varrho(y,z)$ is a smoothed $\varrho(y,z)$, in such a way that roughly all (spatial) frequencies are removed that are higher than $1/\pi y_0$ and $1/z_0$ in the reciprocal y direction and z direction, respectively, but complete information on the more gradual variations in the spin density is still present in ${}_{\mathrm{C}}\varrho(y,z)$ (Appendix B)[7].

In the present case the expansion coefficients in (2.27) do not coincide with the values which ${}_{\mathrm{C}}\varrho(y,z)$ assumes at the lattice points, although these values characterize the function completely. They must therefore be calculated from

$$ {}_{\mathrm{C}}\varrho(n\pi y_0, mz_0) = \sum_{n'=-\infty}^{\infty} \sum_{m'=-M'}^{M'} \frac{{}_{\mathrm{C}}\Psi_{n'm'}(n\pi y_0, mz_0)}{y_0 z_0}\, {}_{\mathrm{C}}\mathscr{P}_{n'm'}, \tag{2.29} $$

which can be regarded as a filtering of $\{{}_{\mathrm{C}}\mathscr{P}_{nm}\}$. The computer simulation results in Figs. 2c and d demonstrate the combined effect of the transformations given by (2.26) and (2.29) on the spectrum of Fig. 2a. In Fig. 2c ${}_{\mathrm{C}}\varrho(n\pi y_0, mz_0)$ is shown as a function of $nM+m$ and this is converted into an intensity plot in Fig. 2d. The spurious feature has fully disappeared and only a bright spot at the correct position $(5\pi y_0, 2z_0)$ has remained.

We have found that cosine-wave modulation of the gradient fields also yields a signal that contains the desired information on the spin density, but that a rather complex transformation is needed to get this information in a convenient form. In particular, all spectral coefficients ${}_{\mathrm{C}}\mathscr{M}_{n'M+m}$ with $|n'| \lesssim |n|$ make important contributions to the spin density at the lattice point $(n\pi y_0, mz_0)$. It will further be clear that the filter operation cannot be avoided in the case of cosine-wave modulation, not even at the expense of specimen size. Again, relaxation causes broadening in the z direction. Near the edges $z \approx \pm M'z_0$ we have transfer of intensity to the opposite side of the picture as in the square wave case, but the ensuing redistribution in the y direction of the transferred intensity is not so easy to describe due to the complexity of the transformation involved.

3. Signal Sampling

We shall describe what has to be changed in the treatment above if the FID signal is sampled and not recorded continuously as we have assumed until now. As is well known [17], by introducing a shortest time interval Δt and thus a largest frequency difference $1/\Delta t$ sampling causes aliasing in the spectrum: any frequency higher than $1/2\Delta t$ is folded back to a frequency lower than $1/2\Delta t$ so that these become indistinguishable. Since NMR frequency corresponds to distance in the specimen through the gradient fields, it is to be expected that sampling will set an upper limit to the allowable specimen size.

We consider the situation where $m_+(t)$ is sampled at the instants between 0 and T that are integral multiples of T/L, where $L=NM$ and N is an integer, which we assume to be odd and write as $N=2N'+1$. Discrete Fourier transformation now yields

$$ \mathscr{M}_k^{(2L)} = \frac{1}{2L} \sum_{j=-L}^{L-1} m_+(jT/L) \mathrm{e}^{-\mathrm{i}kj\pi/L} = \iint \varrho(y,z) \Phi_k^{(2L)}(y,z)\,\mathrm{d}y\,\mathrm{d}z, \quad k=-L,\ldots,L-1, \tag{3.1} $$

where

$$ \Phi_k^{(2L)}(y,z) = \sum_{l=-\infty}^{\infty} \Phi_{k+l2L}(y,z) = \sum_{n=-N}^{N-1} \alpha_n^{(2N)}(y) \beta_{k-nM}^{(2L)}(z), \tag{3.2} $$

[7] See footnote on p. 258.

with analogous definitions of the functions $\alpha_n^{(2N)}$ and $\beta_m^{(2L)}$ as infinite sums of their non-superscripted counterparts. So again we obtain weighted integrals of the spin density distribution, this time with respect to a set of modified weight functions $\{\Phi_k^{(2L)}(y,z)\}$, which moreover is finite. With (3.1) and (3.2) replacing (1.7) and (1.8) the entire further analysis now proceeds in exactly the same way as discussed in the previous sections. Therefore we shall only state the main results and comment on them briefly.

3.1. Square Wave Modulation

For the expansion of the spin density the following functions are used:

$$ {}_{\mathrm{S}}\Psi_{nm}^{(2L)}(y,z)=w_n^{(N)}(y/2y_0+(z/z_0-m)/2M)w_m^{(M)}(z/z_0), $$
$$ m=-M',\ldots,M', \quad n=-N',\ldots,N'. \tag{3.3} $$

The filtering of the spectrum is given by

$$ {}_{\mathrm{S}}\mathscr{P}_{nm}^{(2L)}={}_{\mathrm{S}}\mathscr{M}_{2nM+m}^{(2L)}+\sum_{n'=-N'}^{N'} S_{nn'}^{(N)}\,{}_{\mathrm{S}}\mathscr{M}_{(2n'-1)M+m}^{(2L)}, \tag{3.4a} $$

$$ S_{nn'}^{(N)}=\frac{(-1)^{n-n'}}{N\sin[(n-n'+\frac{1}{2})\pi/N]}=w_0^{(N)}(n-n'+\tfrac{1}{2}), \tag{3.4b} $$

and the desired representation of the spin density distribution takes the form

$$ {}_{\mathrm{S}}\bar{\varrho}(y,z)=\frac{1}{2y_0z_0}\sum_{n=-N'}^{N'}\sum_{m=-M'}^{M'} {}_{\mathrm{S}}\mathscr{P}_{nm}^{(2L)}\,{}_{\mathrm{S}}\Psi_{nm}^{(2L)}(y,z). \tag{3.5} $$

Because of the periodicities in the functions ${}_{\mathrm{S}}\Psi_{nm}^{(2L)}(y,z)$ this representation is only unambiguous if the size of the specimen is such that $y<Ny_0$ and $Z<Mz_0/2$.

The functions ${}_{\mathrm{S}}\Psi_{nm}^{(2L)}(y,z)$ are orthogonal on the rectangle $-Ny_0\leqq y\leqq Ny_0$, $-Mz_0/2\leqq z\leqq Mz_0/2$, they form a semicomplete set with spacings $2y_0$ and z_0, and they are orthonormal with respect to a discrete inner product on the corresponding enclosed lattice. The semicompleteness implies

$$ {}_{\mathrm{S}}\bar{\varrho}(y,z)=\frac{1}{2y_0z_0}\iint\varrho(y+y',z+z')\cdot w_0^{(N)}(y'/2y_0+z'/2Mz_0)w_0^{(M)}(z'/z_0)dy'dz', \tag{3.6} $$

which demonstrates once more the necessity of limits on the specimen size. The expansion coefficients ${}_{\mathrm{S}}\mathscr{P}_{nm}^{(2L)}$ are directly proportional to the values of ${}_{\mathrm{S}}\bar{\varrho}(y,z)$ at the lattice points $(n2y_0,mz_0)$.

We remark that the computer simulation results shown in Fig. 1 were of course obtained with the transformations just described, involving only a finite number of weighted integrals, expansion coefficients, and so on.

The doubling of the available amount of information by the filter may now be formulated as follows. Sampling of the FID signal at L instants between 0 and T provides us with L complex numbers $m_+(jT/L)$, which are converted into $2L$ real weighted integrals ${}_{\mathrm{S}}\mathscr{M}_k^{(2L)}$. With the transformation given by (3.4) we extract from them L independent values of the spin density at L lattice points in the rectangle $-Ny_0\leqq y\leqq Ny_0$, $-Mz_0/2\leqq z\leqq Mz_0/2$. (As we do not use the possibility to construct a second set of functions from the ${}_{\mathrm{S}}\Phi_k^{(2L)}(y,z)$ because of numerical difficulties, the number of independent data is reduced by a factor of 2 here.) Without the transformation we would have to require that $\varrho(y,z)$ be zero for $y<0$. Since only half of the remaining ${}_{\mathrm{S}}\mathscr{M}_{nM+m}^{(2L)}$ would then be independent, we would end up with $\frac{1}{2}L$ independent values of the spin density at $\frac{1}{2}L$ lattice points in the rectangular area $0\leqq y\leqq Ny_0$, $-Mz_0/2\leqq z\leqq Mz_0/2$.

3.2. Cosine Wave Modulation

The functions involved in the expansion of the spin density are

$$ \begin{aligned} {}_{\mathrm{C}}X_{nm}^{(2L)}(y,z)&=\sum_{l=-N}^{N-1}K_{n+l/2}^{(N)}(y/y_0)w_{m-lM}^{(2L)}(z/z_0)\\ &=K_{n-(z/z_0-m)/2M}^{(N)}(y/y_0)w_m^{(M)}(z/z_0),\\ &\quad m=-M',\ldots,M', \quad n=-N',\ldots,N', \end{aligned} \tag{3.7} $$

and

$$ \begin{aligned} {}_{\mathrm{C}}\Psi_{nm}^{(2L)}(y,z)&=\sum_{l=-N}^{N-1}F_{n+l/2}^{(N)}(y/y_0)w_{m-lM}^{(2L)}(z/z_0)\\ &=F_{n-(z/z_0-m)/2M}^{(N)}(y/y_0)w_m^{(M)}(z/z_0),\\ &\quad m=-M',\ldots,M', \quad n=-N',\ldots,N'. \end{aligned} \tag{3.8} $$

The spectrum must be subjected to the same filter as in the square-wave case,

$$ {}_{\mathrm{C}}\mathscr{P}_{nm}^{(2L)}={}_{\mathrm{C}}\mathscr{M}_{2nM+m}^{(2L)}+\sum_{n=-N'}^{N'} S_{nn'}^{(N)}\,{}_{\mathrm{C}}\mathscr{M}_{(2n'-1)M+m}^{(2L)}, \tag{3.9} $$

and the spin density distribution is represented as

$$ {}_{\mathrm{C}}\bar{\varrho}(y,z)=\frac{1}{y_0z_0}\sum_{n=-N'}^{N'}\sum_{m=-M'}^{M'} {}_{\mathrm{C}}\mathscr{P}_{nm}^{(2L)}\,{}_{\mathrm{C}}\Psi_{nm}^{(2L)}(y,z), \tag{3.10} $$

which is unambiguous if the specimen dimensions satisfy $Y\lesssim Ny_0$ and $Z<Mz_0/2$.

There is a mathematical complication here. Although the sets $\{{}_{\mathrm{C}}X_{nm}^{(2L)}\}$ and $\{{}_{\mathrm{C}}\Psi_{nm}^{(2L)}\}$ contain only a finite number of functions they do not form an exactly biorthogonal system on any finite area, essentially because they are not periodic in the y variable (Appendix B)[8]. Yet for practical purposes it is sufficient that the system built up from $\{{}_{\mathrm{C}}X_{nm}^{(2L)}\}$ and $\{{}_{\mathrm{C}}\Psi_{nm}^{(2L)}\}$ is *approximately* biorthogonal on the rectangle

[8] See footnote on p. 258.

$-Ny_0 \leqq y \leqq Ny_0$, $-Mz_0/2 \leqq z \leqq Mz_0/2$, and is also *approximately* semicomplete with spacings πy_0 and z_0. The representation defined by (3.10) in fact satisfies

$$ {}_C\bar{\varrho}(y,z) = \frac{1}{y_0 z_0} \iint \varrho(y+y', z+z') \cdot F^{(N)}_{-z'/2Mz_0}(y'/y_0) w_0^{(M)}(z'/z_0) dy' dz' , \tag{3.11} $$

from which it may be appreciated, in view of the shape of the functions $F_\nu^{(N)}(\,.\,)$ and $w_0^{(M)}(\,.\,)$, that ${}_C\bar{\varrho}(y,z)$ images the more gradual variations in the spin density accurately if the specimen size falls well within the limits given above.

4. Resolution and Allowable Specimen Size

We are now in a position to discuss how important characteristics of the method, such as attainable resolution and maximum allowable specimen size, are connected with the various experimental parameters. We only consider gradient modulation as described in Sect. 2.

The resolutions Δy and Δz in the directions of the orthogonal gradients, when identified with the lattice spacings associated with semicompleteness, turned out to be of the order of $y_0 = \omega_1/\gamma G_y$ and $z_0 = \Omega/\gamma G_z$, respectively. Thus the resolution is largely determined by the quotient of modulation frequency and gradient strength, and the precise form of the modulation pattern has only a minor effect on it. For the z direction, where the gradient is steady, it is useful to write $\Delta z = z_0 = \pi/\gamma G_z T$, which shows the size of the smallest resolvable detail to be inversely proportional both to gradient strength and to measuring time. In the y direction, corresponding to the gradient that is actually modulated, we have $\Delta y = 2y_0$ for a square-wave modulation pattern and $\Delta y = \pi y_0$ for cosine-wave modulation. We point out that when expressed in terms of an *effective* gradient strength

$$ \bar{G}_y = \frac{\omega_1}{2\pi} \int_0^{2\pi/\omega_1} G_y |f_1(t)| dt \tag{4.1} $$

by which ${}_S\bar{G}_y = G_y$ and ${}_C\bar{G}_y = 2G_y/\pi$, the resolution is equal to $2\omega_1/\gamma\bar{G}_y$ for *both* modulation patterns. This is worse by a factor of 2 compared to the resolution obtained with a steady gradient. Finally, it will be clear that if one gradually smoothes the square wave form until it has changed into a cosine wave form the resolution will change monotonously from $2y_0$ to πy_0.

The size of the specimen in the z direction, $2Z$, is not allowed to exceed $Mz_0 = \omega_1/\gamma G_z$. Thus, when measured in units of resolution it is limited by the ratio $M = \omega_1/\Omega = \omega_1 T/\pi$, i.e. twice the number of modulation periods of the y gradient during the measuring time. Therefore, if T is fixed, the allowable specimen size can be increased in the z direction at constant resolution Δz by an increase of ω_1, which, however, causes the resolution in the y direction to deteriorate proportionally, unless the strength of the y gradient is also increased. Of course, it is always possible to relax the limit on $2Z$ at the expense of resolution in the z direction by a reduction of the gradient strength G_z.

The size of the specimen in the y direction, $2Y$, is in principle not limited by the method but only by the size of the measuring apparatus. However, if the FID signal is sampled, the sampling rate NM/T sets an upper limit $2Ny_0 = (NM/T)2\pi/\gamma G_y$ to $2Y$. That is N units of resolution in the square-wave case, $2N/\pi$ units in the cosine-wave case.

We have collected these results in Table 1. It is now easy to compare the performance of square-wave modulation with that of cosine-wave modulation in the situation where all experimental parameters are the same. We have seen that both modulation patterns allow the same specimen size but that the resolution is better by a factor of $\pi/2$ with square-wave modulation, and accordingly the number of independent data points is larger by that factor (compare Figs. 1d and 2d, noting that N is twice as large in Fig. 2). Expressed in units involving the effective gradient strength it is the specimen size that is larger by a factor of $\pi/2$ in the square-wave case, while the resolution is the same for both modulation patterns.

Table 1. Dependence of resolution and allowable specimen size on experimental parameters. Here G_y and G_z are the gradient strengths, $\Omega = \pi/T$ where T is the measuring time, $\omega_1 = M\Omega$ is the modulation circular frequency, and NM/T is the sampling rate

	z direction (static gradient)	y direction (with square-wave modulation)	y direction (with cosine-wave modulation)
Resolution	$\Omega/\gamma G_z$	$2\omega_1/\gamma G_y$	$\pi\omega_1/\gamma G_y$
Maximum specimen dimension	$M\Omega/\gamma G_z$	$N\,2\omega_1/\gamma G_y$	$N\,2\omega_1/\gamma G_y$
Number of points resolved	M	N	$2N/\pi$

Finally, we show how the present treatment can be extended to the situation where B_2 is periodic. Let ω_2 be the circular frequency of the B_2 modulation. First, we consider the case where ω_1 is an integral multiple of ω_2. Now notice that in the foregoing formalism the quantity Ω has acted in many respects as a circular frequency associated with B_2, because $2\pi/\Omega = 2T$ is the time during which B_2 is effective. We might as well view this time interval as the first single period of a field that is continued periodically. Therefore the case $\omega_1 = M\omega_2$, where M is an integer, is already covered by the formulation above if only Ω is replaced by ω_2 everywhere and the appropriate time dependence of B_2 is inserted in (1.2) and used in the evaluation of $\beta_m(z)$.

Second, we demonstrate that a rational frequency ratio is not fundamentally different from an integral frequency ratio, so that our assumption above caused no loss of generality. Let us suppose that $M_2\omega_1 = M_1\omega_2$, with $M_1 > M_2$ (in this notation we had $M_1 = M$ and $M_2 = 1$ up to now). The effective measuring time $2T$ must then be $2T = M_2 2\pi/\omega_2 = M_1 2\pi/\omega_1$ in order that the measurement effectively lasts an integral number of full periods of each modulation field. Since more than one period of the field B_2 is now necessarily involved we must exclude the presence of any time-independent part in B_2 in order that φ_2 is zero at the beginning of each period.

For the sake of the argument assume square-wave modulation for both gradient fields. Analogous to our previous derivation one readily finds that the weight functions $\Phi_k(y, z)$ appearing in the weighted integrals of $\varrho(y, z)$ are in this case given by

$$\Phi_{nM_1+mM_2}(y,z) = \sum_{l=-\infty}^{\infty} v_{n+lM_2}(y/2y_0)v_{m-lM_1}(z/2z_0), \quad (4.2)$$

where k is uniquely decomposed as $k = nM_1 + mM_2$ by the requirement that $0 \leqq m \leqq M_1 - 1$. From (4.2) we appreciate that after a double filter transformation so as to remove spurious reflections in both directions we are left with resolutions $\Delta y = 2\omega_1/\gamma G_y$ and $\Delta z = 2\omega_2/\gamma G_z = 2M_2\pi/\gamma T G_z$ and maximum allowable specimen dimension $2Z = M_1\omega_2/\gamma G_z = M_1 M_2 \pi/\gamma T G_z$. Comparison with Table 1 shows that for fixed T almost nothing is gained by having both gradient fields modulated instead of one. The allowable specimen dimension $2Z$ can be increased by an increase of ω_2, but Δz increases proportionally so that the number of independent data points in the z direction does not change with ω_2 but is still determined by ω_1. The additional flexibility that $2Z$ and Δz can be varied not only through G_z but also through ω_2 is paid for by the disadvantageous factor 2 in the expression for Δz. This factor stems from B_2 being actually modulated instead of being kept steady.

5. Practical Considerations

Anticipating conclusions presented later in this section, we can say that an approximately square-wave modulation meets insurmountable practical difficulties. It is the high rate of magnetic field variation which we expect to cause trouble, in particular for such applications as human-body spin imaging. We limit ourselves, therefore, to cosine-wave modulation.

As a further limitation we shall consider only two-dimensional imaging, since we can state, anticipating again, that the three-dimensional version of the method is realistic only for a very limited resolution, e.g. 8 independent data points in each direction. As noted before, the application of the two-dimensional version is not limited to two-dimensional objects. It can well be applied in a three-dimensional specimen, namely if the method is combined with selective excitation or selective saturation [2, 6, 9, 14].

For a description of practical aspects we adopt the following starting point. We take $2Z$, $2Y$, Δz, Δy, and T as five given quantities. In other words: we have a given specimen of dimensions $2Z$ and $2Y$, and we want resolutions Δz and Δy in the z and y direction, respectively. In practice, the measuring time T is in so far a given quantity as a good choice of its value is dictated by the remaining inhomogeneity ΔB of the background field, this latter field being the strong static field $\mathbf{B}_0$ that remains if the currents through all gradients coils are zero. In order to avoid appreciable distortions (of order Δz) in the image the measuring time T should not much exceed $\pi/\gamma\Delta B$. The value of T is of course also limited by the relaxation times T_2 that occur in the specimen. The part of the sample having relaxation times shorter than the chosen value for T should be negligible, say 5% or less.

In Table 2 we have summarized how various experimental parameters are expressed in terms of $2Z$, $2Y$, Δz, Δy, and T. These expressions are readily derived from Table 1 in Sect. 4.

Table 2. Dependence of the gradient parameters and of the sampling frequency on the specimen dimensions ($2Z$ and $2Y$), the required resolutions (Δz and Δy), and the chosen measuring time T. The y gradient is assumed to vary sinusoidally

z gradient:	$G_z = \dfrac{\pi}{\gamma T \Delta z}$
y gradient modulation frequency:	$\omega_1/2\pi = \dfrac{1}{2T} \cdot \dfrac{2Z}{\Delta z}$
Amplitude of y gradient:	$G_y = \dfrac{\pi^2}{\gamma T \Delta y} \cdot \dfrac{2Z}{\Delta z}$
Maximum rate of field variation:	$\left(\dfrac{dB}{dt}\right)_{\max} = \dfrac{\pi^3}{2\gamma T^2} \cdot \dfrac{2Y}{\Delta y} \cdot \left(\dfrac{2Z}{\Delta z}\right)^2$
Sampling frequency:	$\nu_{\text{sampling}} = \dfrac{\pi}{2T} \cdot \dfrac{2Y}{\Delta y} \cdot \dfrac{2Z}{\Delta z}$

As an example we assume an inhomogeneity $\Delta B = 0.5\,\mu T$ (5 mG) so that $T = 16$ ms is a reasonable choice. Further we assume a sample of 32 cm × 32 cm and we require a resolution of $\Delta z = \Delta y = 1.0$ cm. Using Table 2 one derives for this example

$$G_z = 73\,\mu T/m\ (7.3\,mG/cm),$$

$$\omega_1/2\pi = 1.00\,kHz,$$

$$G_y = 7.3\,mT/m\ (0.73\,G/cm),$$

$$\left(\frac{dB}{dt}\right)_{max} = 7.4\,T/s\ (74\,kG/s),$$

and

$$\nu_{sampling} = 100\,kHz.$$

(In this example we have $M = 32$ and $N = 50$.)

The required homogeneity is not easy to attain in a 32 cm × 32 cm layer and the realization of 7.3 mT/m for G_y is also difficult if a good linearity of the gradient is required.

The rate of magnetic field variation, 7.4 T/s, is already larger than what Budinger [18] judges to be harmless for the human body. For an improved resolution $\Delta z = \Delta y = 0.5$ cm, the values for Z, Y, and T remaining the same, dB/dt has to be eight times larger, 59 T/s.

The sampling frequency need not to be a great problem, not even at $\Delta z = \Delta y = 0.5$ cm, since 400 kHz sampling rate is within the reach of modern minicomputers.

The following remark can be made about the required linearity of the y gradient. Since the two gradient fields affect the spectrum differently because of their different time dependence, it is only the resolution in the y direction and not that in the z direction which determines to what extent the y gradient field may deviate from its ideal form. Thus, time-dependent deviations of order $0.5\,G_y \Delta y \cos\omega_1 t$ are allowed, because such a deviation corresponds to a displacement of a data point by $0.5\,\Delta y$ in the y direction. Only static deviations could disturb the resolution in the z direction and should be smaller than $0.5\,G_z \Delta z$.

Mansfield [8] has remarked that one may take the strong gradient as the fixed one and vary the small gradient periodically, provided that one applies 180° time-reversing pulses. In a two-dimensional sample this might be realistic but for imaging a selected layer of a three-dimensional specimen it is not yet clear how one should do this. Good selective 180° pulses are for instance not yet known [14]. Therefore the required strength G_y of the modulated gradient seems to be the major technical limiting factor.

In conclusion we think that the example above is certainly difficult to realize but would still be just attainable. The echo planar imaging method has thus a limited resolution, but 32×32 independent image points may yet contain enough information in certain applications.

6. Summary and Conclusions

We have derived a general formalism for the analysis of NMR spin imaging spectra obtained with magnetic field modulation during the free induction decay. We have shown that this technique yields weighted integrals of the spin density distribution. The information contained in these integrals depends upon the weight functions, which in turn are determined completely by the spatial dependence and the modulation pattern of the modulated magnetic fields. This insight led to a prescription for reconstructing the spin density distribution from the measured FID signal.

We have applied the formalism to two-dimensional imaging with one static and one modulated magnetic gradient field. The solution to the image reconstruction problem then consists in the application of a filter to the FID spectrum. For the cases of square-wave and cosine-wave modulation we have given explicit expressions for these reconstructing filters and demonstrated their effect in computer-simulated pictures. In the case of square-wave modulation one could try to avoid use of the filter but this would be at the expense of half of the space available for the specimen. With cosine-wave modulation the filter transformation is indispensable for getting an unambiguous image at all.

An analysis of the attainable resolution and allowable specimen size gave the following results. For gradient strengths G_z (static) and G_y (modulated), modulation frequency $\omega_1/2\pi$, measuring time $T = M\pi/\omega_1$, and sampling rate $\nu = NM/T$ the resolution Δz in the direction of the static gradient is equal to $\pi/\gamma T G_z$, the resolution Δy in the direction of the modulated gradient is $2\omega_1/\gamma G_y$ for square-wave modulation or $\pi\omega_1/\gamma G_y$ for cosine-wave modulation, and the maximum allowable specimen dimensions are $M\pi/\gamma T G_z$ and $2N\omega_1/\gamma G_y$. We then argued that three-dimensional imaging by the present method is realistic only for a very limited resolution. However the method can be quite useful for two-dimensional imaging of a selected layer in a three-dimensional object. A resolution of 1 cm × 1 cm in a 32 cm × 32 cm specimen would be attainable, although it will be difficult to achieve this in practice. In particular a rather high value for G_y is required. For medical applications the high rate of magnetic field variation may be a limiting factor.

Acknowledgements. We would like to thank T. A. C. M. Claasen, W. F. G. Mecklenbräuker, and D. Polder for stimulating discussions, and K. Weiss and R. Rieckeheer for valuable comments on the manuscript.

References

1. P.C.Lauterbur: Pure Appl. Chem. **40**, 149–157 (1974)
2. A.N.Garroway, P.K.Grannell, P.Mansfield: J. Phys. C **7**, L 457–L 462 (1974)
3. A.Kumar, D.Welti, R.R.Ernst: J. Magn. Reson. **18**, 69–83 (1975)
4. W.S.Hinshaw: J. Appl. Phys. **47**, 3709–3721 (1976)
5. R.Damadian, L.Minkoff, M.Goldsmith, M.Stanford, J.Koutcher: Science **194**, 1430–1432 (1976)
6. P.Mansfield, A.A.Maudsley: J. Magn. Reson. **27**, 101–119 (1977)
7. P.Mansfield: J. Phys. C **10**, L 55–L 58 (1977)
8. P.Mansfield, I.L.Pykett: J. Magn. Reson. **29**, 355–373 (1978)
9. J.M.S.Hutchison, R.J.Sutherland, J.R.Mallard: J. Phys. E **11**, 217–221 (1978)
10. W.S.Hinshaw, E.R.Andrew, P.A.Bottomley, G.N.Holland, W.S.Moore, B.S.Worthington: Br. J. Radiol. **52**, 36–43 (1979)
11. D.I.Hoult: J. Magn. Reson. **33**, 183–197 (1979)
12. P.Brunner, R.R.Ernst: J. Magn. Reson. **33**, 83–106 (1979)
13. W.S.Hinshaw: Phys. Lett. A **48**, 87–88 (1974)
14. P.R.Locher: Phil. Trans. R. Soc. London Ser. B, in press (1980)
15. P.M.Morse, H.Feshbach: *Methods of Theoretical Physics*, Part I (McGraw-Hill, New York 1953) pp. 928–931
16. M.Abramowitz, I.A.Stegun: *Handbook of Mathematical Functions* (National Bureau of Standards, Washington 1964) Chap. 9
17. T.C.Farrar, E.D.Becker: *Pulse and Fourier Transform NMR* (Academic Press, New York 1971) pp. 70–71
18. T.F.Budinger: IEEE Trans. Nucl. Sci. NS-**26**, 2821–2825 (1979)